https://doi.org/10.3311/PPci.22324

Periodica Polytechnica Civil Engineering

Shear Strength Evaluation of Concrete Beams with FRP Transverse Rebar

Gökhan Barış Sakcalı[1*], İsa Yüksel[1]

[1] Department of Civil Engineering, Faculty of Engineering and Natural Sciences, Bursa Technical University, Mimar Sinan Campus, 16330, Bursa, Turkey
[*] Corresponding author, e-mail: gokhan.sakcali@btu.edu.tr

Received: 03 April 2023, Accepted: 18 October 2023, Published online: 02 January 2024

Abstract

Rebar corrosion in traditional reinforced concrete (RC) components may lead to a decrease in service life and carrying capacity. This condition is one of the reasons of the growing popularity of Fiber Reinforced Polymer (FRP) rebars as a corrosion-resistant alternative, particularly in RC infrastructure projects. Because the material properties and behavior of FRP rebar are very different from conventional steel rebar, the calculations used for reinforced concrete with conventional steel reinforcement should be updated for this material. The aim of this study is to propose a new shear strength prediction model for RC beams with transverse steel rebar in order to calculate the shear strength of RC beams with FRP transverse rebar according to TS-500, which is the Turkish Building Code. To achieve this goal, Finite Element Method (FEM) models were created for 27 RC beams with FRP transverse rebars and 9 RC beams without transverse rebars. Furthermore, for RC beams with FRP transverse rebars, a prediction model has been developed. Additionally, 13 prediction models obtained from regulations or scientific studies were compared to the proposed prediction model using a database of 105 tests obtained from previous experimental studies. It was observed that the proposed prediction model provides more consistent results with the test database from the literature compared to the models suggested by other regulations or studies. Therefore, by modifying the shear strength relations recommended in TS-500 for RC beams with transverse steel rebar, they can also be applied to RC beams with transverse FRP rebars.

Keywords

FRP rebars, RC beam, shear strength, stirrup

1 Introduction

Rebar corrosion is a common issue in Reinforced Concrete (RC) structures located in corrosive environments. Corrosion degradation negatively impacts the structural behavior and significantly reduces the service life of RC structures. Therefore, the assessment of serviceability and structural performance in RC structures, which often involves additional expenses, must take into consideration the time-dependent variations in structural responses [1]. In this context, a notable advantage is that the strength of RC elements with FRP rebar remains relatively unchanged even after years. In highly corrosive environments, it often makes more sense to prefer Fiber Reinforced Polymer (FRP) composite rebar due to its superior corrosion resistance, as opposed to traditional steel rebar. Besides it's corrosion resistance, Fiber Reinforced Polymer (FRP) rebar offers several superior properties compared to conventional steel rebar, such as excellent corrosion resistance, lightweight characteristics, non-conductivity, limited thermal expansion, high strength, and effective damping properties. While the use of FRP materials as reinforcement dates back to the mid-1980s [2], the first application of FRP reinforcing bars can be traced to the mid-1990s. Nowadays, FRP sheet, FRP plate and FRP rebar materials are frequently used in the design or strengthening [3] of RC elements. Reliability-based design of beams produced using FRP material has emerged as an important research topic in recent years [4, 5].

The shear strength of RC elements with FRP longitudinal reinforcement and without transverse reinforcement is influenced by parameters such as aggregate size in concrete, material strengths of concrete and rebar, section geometry, shear span to depth ratio of beam (a/d), and reinforcement ratio. When considering RC elements with stirrups, it's important to include parameters such as the spacing and diameter of transverse rebar, in addition to the material properties of transverse rebar.

Cite this article as: Sakcalı, G. B., Yüksel, İ. "Shear Strength Evaluation of Concrete Beams with FRP Transverse Rebar", Periodica Polytechnica Civil Engineering, 2024. https://doi.org/10.3311/PPci.22324

The neutral axis depth in conventional RC members increases more with the yielding of the steel rebar. However, as the FRP rebar is ruptured without yielding, the compression zone depth does not change much with the increasing load [6, 7]. Furthermore, compared to conventional RC members, the contribution of dowel action may be smaller with FRP rebar than with steel rebar, due to the anisotropic structure of FRP rebar and the wider cracks observed in RC members with FRP rebar. There is also the complex stress state resulting from the fibers kinking at the corner where the stirrup bends. These situations lead to distinct shear behaviors in RC elements with FRP rebar compared to conventional RC elements. For these reasons, the use of models that disregard the properties of FRP rebars in the design phase may result in calculation errors and structural failures. Moreover, the development of predictive models for the shear strength of RC beams containing FRP transverse rebars may lead to the design of RC elements that are impervious to corrosion.

The shear behavior of RC members has a complex structure, and there is a need for new design proposals to reveal the shear behavior of RC members with FRP rebar better. In the last few decades, various researchers have proposed different prediction models to calculate the shear strength of FRP-RC members without stirrups. Moreover, some regulations and researchers have proposed prediction models for the shear strength of RC members with FRP stirrups [6–18]. In many countries, when RC is mentioned, steel-reinforced RC comes to mind and regulations are formulated accordingly. However, in some regulations, specific equations are given for the conventional RC, taking different properties and behaviors of FRP rebar into account. Current calculation and design regulations in Türkiye, such as TS-500 [19] and TBEC-2018 [20], have been prepared considering RC members with only steel rebar.

Today, FRP rebar types are used in various infrastructure constructions and it is expected that the use of this type of rebar will become widespread in the future. As such, standards or regulations will need to be updated to include FRP rebar. In the past, only conventional steel rebar was used as rebar in reinforced concrete (RC) structures. Therefore, in many countries, RC calculation methods and related standards were primarily developed with a focus on steel reinforcement. However, today, Fiber-Reinforced Polymer (FRP) reinforcement is also used, especially in infrastructure construction, and it is anticipated that it's use will continue to grow. Therefore, it is necessary to update existing RC calculation methods to accommodate FRP rebars.

The goal of this study is to evaluate current prediction models for the shear strength of concrete beams incorporated with FRP transverse rebar and to propose a new prediction model. For this purpose, a series of numerical studies have been carried out, and accordingly, a 3D finite element model of 27 concrete beams with FRP transverse rebar, and 9 concrete beams without transverse rebar have been computerized, respectively. Based on these models, the shear strength equations given for conventional RC beams in TS-500 [19], Turkish Reinforced Concrete Regulation, is revised and recommended for use in concrete beams with FRP transverse rebar as well. In addition, 105 test data on the shear strength of RC beams with FRP stirrups in the literature, the prediction models given by different researchers and different regulations were comparatively analyzed with the prediction model proposed in this study [6–18].

2 Materials and methods

2.1 Material properties of GFRP rebar

The tensile strength of GFRP rebar is variable, as production parameters greatly affect the mechanical properties of it. In order to determine Young's Modulus and the tensile strength of the GFRP rebar used in this research, a tensile test was conducted according to the standard ASTM D7205-11 [21]. 5 test specimens were prepared and the specimens were pulled at a loading rate of 0.01 strain/minute. Table 1 shows properties of GFRP rebar prepared for tensile test. Axial strain measurements were obtained

Table 1 Properties of GFRP rebar prepared for tensile testing

Sample	L_a (mm)		L (mm)	t (mm)	Steel tube diameter (mm)		Rebar diameter (mm)
	Left	Right			Left	Right	
A	290	330	350	5.72	31.86	31.90	8.04
B	300	300	360	5.83	31.89	31.89	8.26
C	300	300	368	5.78	31.86	31.86	8.22
D	300	300	372	5.84	31.92	31.43	8.31
E	298	298	371	5.65	31.90	31.94	8.31

L_a: Anchor length, L: Length between anchors, t: Steel tube thickness

using a video extensometer. Since the GFRP rebar slipped from the anchor in the B and E specimens the correct tensile strength values could not be obtained from these specimens. Slippage of this kind did not occur on the other samples (A, C, D). The visuals of the ultimate state of the samples and the test results of the GFRP rebar are presented in Fig. 1 and Fig. 2, respectively.

Tensile strength and Young's Modulus of GFRP rebar in ACI 440R-07 [22] vary between 35000–51000 MPa and 483–1600 MPa, respectively. The mean of Young's Modulus and tensile strength obtained from the test was determined as 41341 MPa and 799 MPa, respectively. This shows that the average value of the properties of the materials is compatible with the values given in ACI 440R-07 [22].

2.2 3D finite element model

It is important to numerically model RC elements to reflect the correct behavior, and three techniques are used to achieve this: discrete, embedded and smeared models. These modelling approaches are predicated on the principle of maintaining the composite continuity between the concrete element group and the rebar element group. Within the scope of this research, the discrete model approach was used in order to reflect the bond strength-slip relationship more accurately and shorten the analysis time.

Although different numerical methods can be used in modelling and analysis of structural elements, the most widely used method is Finite Element Method (FEM). ANSYS [23] software was used in the creation of finite

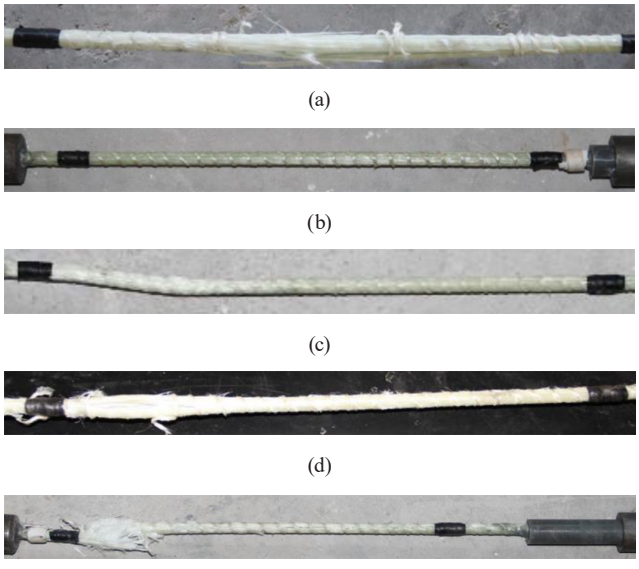

(a)

(b)

(c)

(d)

(e)

Fig. 1 GFRP rebar tensile test visuals; (a) A sample, (b) B sample (slipped), (c) C sample, (d) D sample, (e) E sample (slipped)

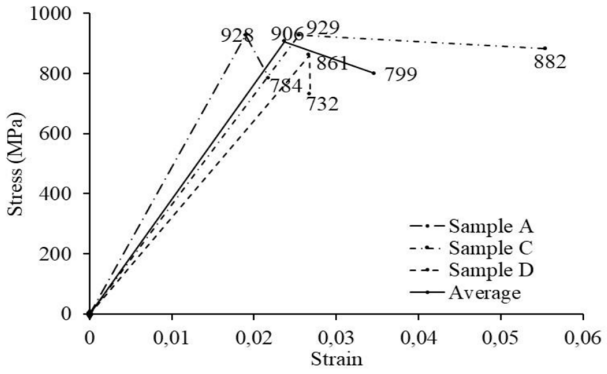

Fig. 2 GFRP rebar tensile test results

element models. Eight-node Solid65 element type was used for modelling three-dimensional concrete elements. By this element type, both the cracking and crushing properties of concrete can be taken into account in the nonlinear behavior of concrete. The compressive strength of concrete (f_c) was used as 40 MPa and the concrete compressive material model was created by Eqs. (1)–(3) [24] (Fig. 3(a)). The first point on the stress-strain curve is defined as 30% of the ultimate compressive strength, considering Hooke's law and Young's Modulus (E_c). Eqs. (4) and (5) were used to determined Young's Modulus [20] and the tensile strength of concrete (f_{cl}), respectively. In addition, Poisson's ratio of concrete is taken into account as 0.2. It is of great importance to define the yield criteria of concrete correctly in order to reflect nonlinear behavior realistically in RC elements. Different yield criteria such as Mohr-Coulomb, Drucker-Prager, Bresler-Pister and Willam-Warnke can be used for brittle or semi-brittle materials like concrete. The Willam-Warnke yield criterion was used in this study since it can take into account the multiaxial stress state as well as cracks and crushing. The yield surface is defined based on the principal stresses and five different parameters in this criterion. The element that exceeds the yield surface, cracks due to tensile stress or is crushed due to compressive stress. Definition of open and closed crack shear transfer coefficients were based on the literature for the determination of the yield surface. In this study, shear transfer coefficients were chosen as 0.2 and 0.8, respectively.

$$f = \frac{E_c \varepsilon}{1 + \left(\frac{\varepsilon}{\varepsilon_0}\right)^2} \text{ for nonlinear region} \tag{1}$$

$$f = E_c \varepsilon \quad \text{for linear region} \tag{2}$$

$$\varepsilon_0 = \frac{2 f_c}{E_c} \tag{3}$$

$$E_c = 5000\sqrt{f_c} \tag{4}$$

$$f_{ct} = 0.64\sqrt{f_c} \tag{5}$$

In numerical models, the material behavior of GFRP rebar is assumed to be linear elastic (as shown in Fig. 3(b)). Poisson's Ratio of GFRP rebar is taken into account as 0.2. The modelling of GFRP rebars utilized the Link180 element type. This element type can accommodate nonlinear material behavior and is equipped with three degrees of freedom at each node, exhibiting uniaxial stress behavior [23].

Eqs. (6)–(7), as modified by Vint [25] specifically for GFRP rebar, were employed to model the bond-slip relationship in RC beams with GFRP rebar. Additionally, the values of s_{max} and τ_{max} were considered as 0.556 mm and 11.26 MPa, respectively [25]. The bond-slip relationship employed at the GFRP rebar-concrete interface is depicted in Fig. 3(c). To accurately represent this relationship, spring elements were defined using the Combin39 element type. This element type connects two joints with a nonlinear spring element, considering the force-displacement relationship [25].

$$\tau = \tau_{max}\left(\frac{s}{s_{max}}\right)^{0.0622} \qquad s \le s_{max} \tag{6}$$

$$\tau = \tau_{max}\left(1 - 0.0131\left(\frac{s}{s_{max}} - 1\right)\right) \qquad s > s_{max} \tag{7}$$

To validate the beam models developed in this study, the following specimens were employed: specimen C216-D1 as tested by Barris et al. [26] (Fig. 4(a)), specimen GGu-10d/3p as tested by Wolanski [27] (Fig. 4(b)), specimen 3-10L as tested by Ovitigala et al. [28] (Fig. 4(c)). The study compared the load-displacement relationships of the numerical models with the experimental test data, as illustrated in Fig. 4. Despite minor discrepancies, it is evident from Fig. 4 that the numerical and experimental test results exhibit compatibility with each other.

2.3 Numerical models

The schematic representation of the 3D numerical models created to examine the shear behaviour of RC beams is shown in Fig. 5. These models are considered as M1 (250 × 500), M2 (250 × 600) and M3 (300 × 600) in order to take the size effect into account (Table 2). The rebars 3ϕ12, 3ϕ14, and 3ϕ16 are taken into account in order to observe the effect of the change in tensile reinforcement ratio in RC beam (Table 2). The compressive strength of FRP rebar is substantially lower than it's tensile strength [29].

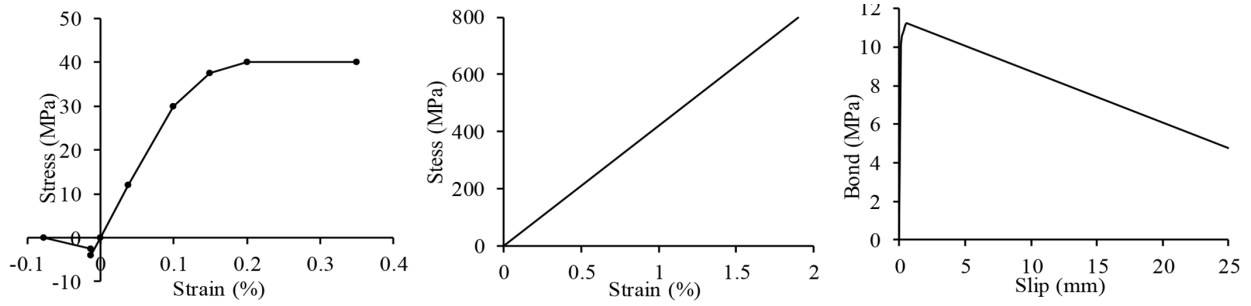

Fig. 3 Models of materials and interface used in analysis, (a) Stress-strain relationship of concrete, (b) Stress-strain relationship of GFRP rebar, (c) GFRP rebar and concrete interface

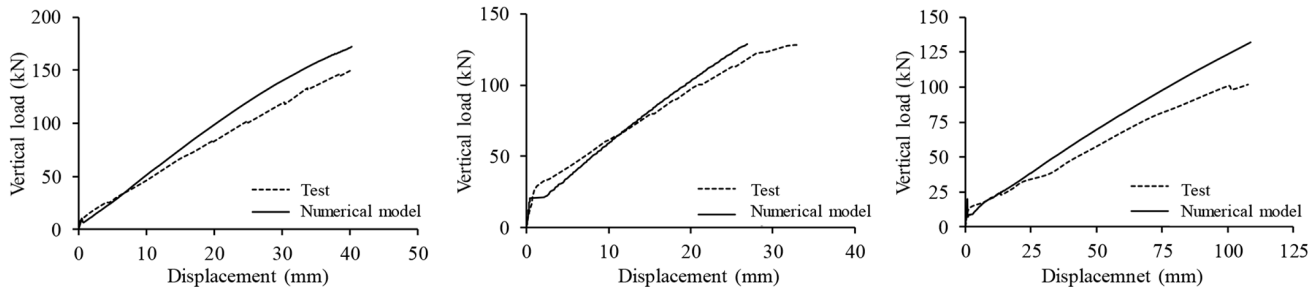

Fig. 4 Comparison of experimental data and numerical models, (a) Sample C216-D1 tested by [26], (b) Sample GGu-10d/3p tested by [27], (c) Sample 3-10L tested by [28]

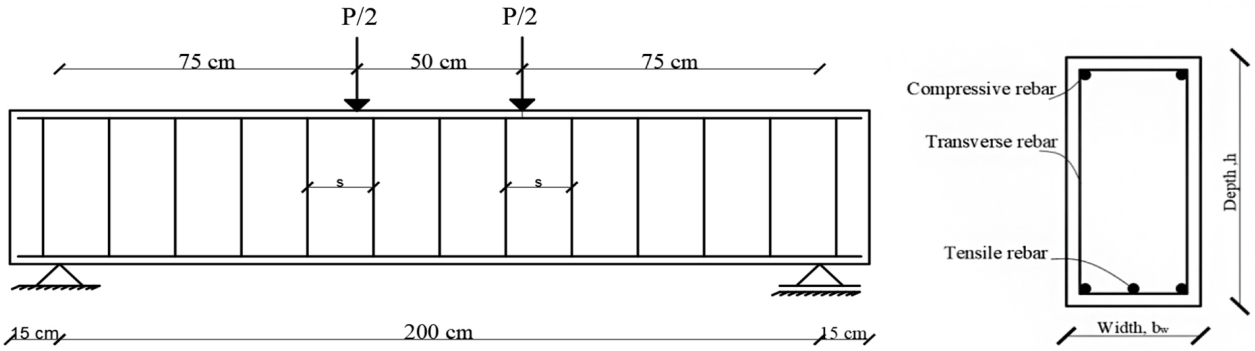

Fig. 5 RC beam with GFRP rebars, (a) Longitudinal cross section, (b) Cross section

Table 2 Properties of RC beams with GFRP rebar

Model code	Width, b_w (mm)	Depth, h (mm)	Tensile rebar	Transverse rebar	Failure load (kN)
M1-0.29-0	250	500	3ϕ12	-	163.99
M1-0.29-0.40	250	500	3ϕ12	ϕ8/100	389.08
M1-0.29-0.27	250	500	3ϕ12	ϕ8/150	316.91
M1-0.29-0.20	250	500	3ϕ12	ϕ8/200	281.42
M1-0.39-0	250	500	3ϕ14	-	164.13
M1-0.39-0.40	250	500	3ϕ14	ϕ8/100	382.44
M1-0.39-0.27	250	500	3ϕ14	ϕ8/150	317.73
M1-0.39-0.20	250	500	3ϕ14	ϕ8/200	280.31
M1-0.51-0	250	500	3ϕ16	-	164.13
M1-0.51-0.40	250	500	3ϕ16	ϕ8/100	381.03
M1-0.51-0.27	250	500	3ϕ16	ϕ8/150	316.81
M1-0.51-0.20	250	500	3ϕ16	ϕ8/200	280.19
M2-0.29-0	250	500	3ϕ12	-	209.74
M2-0.29-0.40	250	600	3ϕ12	ϕ8/100	426.40
M2-0.29-0.27	250	600	3ϕ12	ϕ8/150	390.43
M2-0.29-0.20	250	600	3ϕ12	ϕ8/200	345.47
M2-0.39-0	250	600	3ϕ14	-	209.05
M2-0.39-0.40	250	600	3ϕ14	ϕ8/100	431.91
M2-0.39-0.27	250	600	3ϕ14	ϕ8/150	381.13
M2-0.39-0.20	250	600	3ϕ14	ϕ8/200	344.80
M2-0.51-0	250	600	3ϕ16	-	209.05
M2-0.51-0.40	250	600	3ϕ16	ϕ8/100	421.91
M2-0.51-0.27	250	600	3ϕ16	ϕ8/150	373.50
M2-0.51-0.20	250	600	3ϕ16	ϕ8/200	343.80
M3-0.29-0	300	600	3ϕ12	-	246.03
M3-0.29-0.40	300	600	3ϕ12	ϕ8/100	489.92
M3-0.29-0.27	300	600	3ϕ12	ϕ8/150	429.28
M3-0.29-0.20	300	600	3ϕ12	ϕ8/200	383.55
M3-0.39-0	300	600	3ϕ14	-	246.04
M3-0.39-0.40	300	600	3ϕ14	ϕ8/100	486.51
M3-0.39-0.27	300	600	3ϕ14	ϕ8/150	428.38
M3-0.39-0.20	300	600	3ϕ14	ϕ8/200	374.88
M3-0.51-0	300	600	3ϕ16	-	246.82
M3-0.51-0.40	300	600	3ϕ16	ϕ8/100	489.35
M3-0.51-0.27	300	600	3ϕ16	ϕ8/150	427.41
M3-0.51-0.20	300	600	3ϕ16	ϕ8/200	383.85

Therefore, it is assumed not load-bearing when FRP rebar is used as compression rebar. For this reason, the compression rebar was considered to be 2ϕ8 in all models since it is thought that the change in the compression rebar will not affect the models. Numerical models are modelled with and without transverse rebar. The transverse rebar was chosen as ϕ8/100, ϕ8/150 and ϕ8/200 in RC beams (Table 2). Clear cover of concrete was selected as 25 mm in all models. The numerical models are labelled according to the parameters of cross-section dimension, longitudinal reinforcement ratio ($\rho_f = A_f/b_w d$) and transverse reinforcement ratio ($\rho_{fw} = A_w/b_w s_s$). For example; in the M1-0.29-0.40 model, M1 indicate section size (250 × 500 mm × mm); 0.29 indicate longitudinal reinforcement ratio of 0.29%; and 0.40 indicate transverse reinforcement ratio of 0.40%.

2.4 Prediction model

Shear strength in RC beams is usually expressed by the contribution of five parameters. These are shear strength of concrete (V_c), shear strength of transverse rebar (V_w), shear strength of longitudinal rebar due to dowel action (V_1), the residual tensile strength existing between inclined cracks (V_t), and shear strength due to aggregate interlocking (V_a) (Fig. 6) [6, 30, 31]. The general approach in the proposed shear prediction models is to add the shear strength of the FRP transverse rebars (V_{fw}) to the shear strength of the concrete (V_c), as indicated in Eq. 8. However, in addition to these effects, some researchers [6] and some regulations [10] have taken into account the mechanical interlocking depending on the aggregate size. On the other hand, since the dowel action and the residual tensile strength between the oblique cracks being quite low compared to other contributions, the contribution of the shear strength of the longitudinal rebar was not taken into account in most of the prediction models. In this study, as in many references [7–9, 11–18], it is aimed to develop a prediction model based on TS-500 [19] that takes into account the shear strength provided by concrete and stirrups together.

$$V_r = V_c + V_{fw} \tag{8}$$

The equations given for the concrete shear strength in TS-500 [19] are arranged by considering only the steel rebar (Eq. (9)). Tensile strength of concrete used in the specified equation can be determined using Eq. (10).

$$V_c = 0.65 f_{ct} b_w d \tag{9}$$

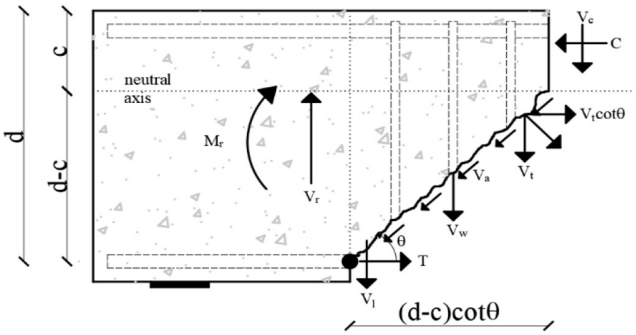

Fig. 6 Shear contributing actions at failure for RC elements with stirrups

$$f_{ct} = 0.35\sqrt{f_c} \tag{10}$$

Recently, the widespread use of RC elements with FRP rebar has made it necessary to revise the equations proposed for RC elements with steel rebars and make them usable for FRP rebar. Some regulations [10–12, 14] and some studies [17, 18] apply a multiplier like Eq. (11) for the effect of FRP rebar on shear strength of concrete. The μ coefficient in Eq. (11) was taken into account as 1/3 by JSCE [11], BISE-99 [12], and Hegger [18], 0.5 by CNR-DT 203 [14] and ISIS-M03-01 [16]. In addition, Nehdi et. al. [17], which made a genetic algorithm-based design proposal, proposed this coefficient as 0.23 for the optimization result and 0.3 for the design.

$$\left(\frac{E_f}{E_s}\right)^{\mu} \tag{11}$$

In this study, it is thought that the concrete shear strength of the RC element with FRP rebar can be determined as in Eq. (12) by integrating Eq. (11) into Eq. (9). Also, in this equation, E_f/E_s ratio should not be greater than 1.0 as in ISIS-M03-01 [16].

$$V_c = 0.65\left(\frac{E_f}{E_s}\right)^{\mu} f_{ct} b_w d \tag{12}$$

Numerical analysis of the RC beams without transverse rebars, the details of which are shown in Table 2, was performed and the concrete shear strength was calculated using prediction model in Eq. (12). The results obtained from the numerical models were curve-fitted depending on the prediction model presented in Eq. (12). As a result, the optimal solution was obtained for the 0.467 value of the μ coefficient. However, for ease of the calculation, the coefficient of μ has been rounded to 0.45. The variation of the ratio of the result obtained from the numerical analysis to the result obtained from the prediction model

(for different coefficient μ) (V_{num}/V_{prep}) depending on the cross-sectional area is given in Fig. 7(a). If the μ coefficient is 0.45, V_{num}/V_{prep} shows that the mean value is about 1.02. This means that the numerical model and the prediction model are quite compatible.

In TS-500 [19], the contribution of transverse rebars to shear strength (Eq. (13)) is evaluated by considering only steel rebar. This equation stated is similar to the equations presented in references JSCE [11], BISE-99 [12], CSA S806-02 [13], ACI 440.1R-06 [15], CNR-DT 203 [14], ISIS-M03-01 [16], Fico et al. [7], Hegger et al. [18], CAN/CSA S806-12 [32], CSA S6-14 [10]. In these references, the equations have been revised to express the contribution of the FRP rebar used as stirrups. Therefore, the equation proposed in TS-500 [19] (Eq. (13)) needs to be revised so that it can be used in stirrups produced from FRP rebar.

$$V_w = \frac{A_w f_{yw} d}{s_s} \tag{13}$$

The stress level in the FRP shear rebar is limited depending on the strain in JSCE [11], BISE-99 [12], ACI440.1R-106 [15], ISIS-M03-01 [16], Hegger et al. [18], CAN/CSA S806-12 [32], and Valivonis et al. [9]. It was emphasized by Fico et al. [7] that the limit strain should vary depending on the type of FRP rebar. The recommended design value of shear rebar strain in ultimate limit state, ε_{fw} values were given as 0.0085, 0.0070 and 0.0035 for GFRP, Aramid Fiber-Reinforced Polymer (AFRP), Carbon Fiber-Reinforced Polymer (CFRP), respectively [7].

The tensile strength of FRP rebar is reduced when bent. For this reason, ACI 440.1R-06 [15] give Eq. (14) for the tensile strength of bent FRP rebar. Thus, the shear crack is controlled and the bent portion of the FRP stirrup failure is prevented. The equation mentioned in ISIS-M03-01 [16] and CSA S6-14 [10] is used more conservatively by dividing it by a coefficient of 1.5.

$$f_{fb} = \left(0.05\frac{r_b}{d_b} + 0.3\right) f_{fu} \le f_{fu} \tag{14}$$

The depth of shear in RC element (d_v) is the distance between the resultants of the compression force and the tensile force due to flexure. ISIS-M03-01 [16], Hegger [18] and CAN/CSA S806-12 [8] have factored the horizontal projection of this distance into their current equations and considered dv as 0.9 d. In CSA S6-14 [10], dv is considered to be greater than 0.9 d and 0.72 h. This is considered by Oller et al. [6] and Cladera et al. [30] as the horizontal projection of the first branch of the critical shear crack.

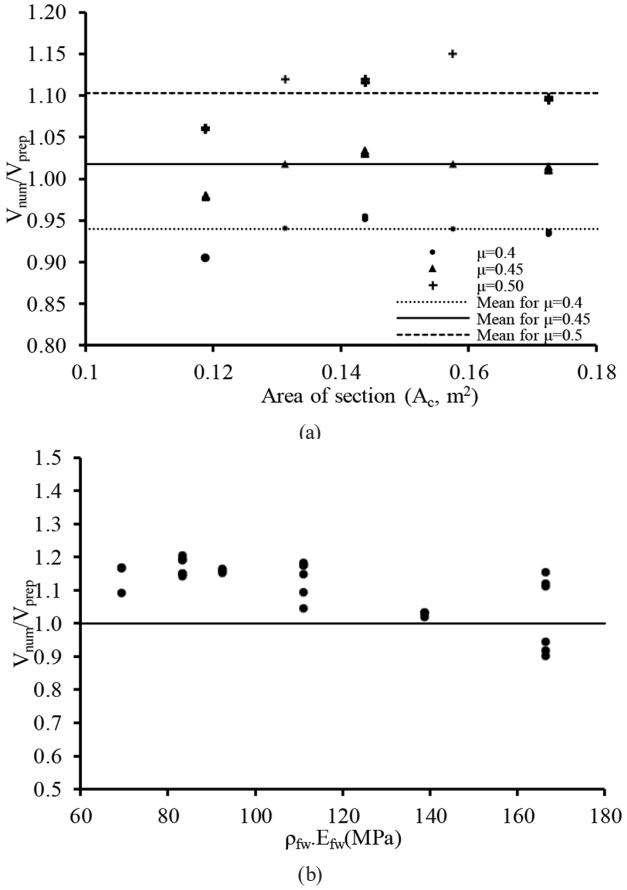

Fig. 7 Variation of V_{num}/V_{prep} according to the cross-sectional area, (a) Comparison according to the shear strength contribution of concrete, (b) Comparison according to the shear strength contribution of transverse rebar

It has been emphasized that this expression can be taken as about equal to 0.85 d.

The existing equation in TS-500 [19] (Eq. (13)) has been proposed by revising it as in Eq. (15). The stirrup stress in this equation can be calculated as in Eq. (16), depending on the strain limit value suggested by Fico et al. [7]. However, in this equation, it is desired to control the shear crack and prevent failure of the FRP stirrup from the bent portion. Therefore, considering the conservative as in ISIS-M03-01 [16], CSA S6-14 [10] and minimum r_b/d_b is 3 as in ACI 440.1R-106 [15], the stress level in the stirrup is limited as in Eq. (16).

$$V_{fw} = \frac{A_w f_{fw} 0.85 d}{s_s} \tag{15}$$

$$f_{fw} = \varepsilon_{fw} E_{fw} \le 0.225 f_{fu} \tag{16}$$

Numerical analysis of RC beams with transverses, the details of which are shown in Table 2, were performed and shear strength of transverse rebar was determined in

these models. The stirrup shear strengths of these models were calculated with the proposed prediction model. From the analysis results, the ratio variation of the result obtained from the numerical model to the proposed prediction model (V_{num}/V_{prep}) according to the reinforcement ratio-Young's Modulus ($\rho_{fw}E_{fw}$) is presented in Fig. 7(b). Also, it was determined that the results obtained from the proposed prediction model could explain 93.7% of the results obtained from the numerical model (R^2 = 93.7%).

2.5 Comparison with test data in the literature

To compare the shear strength of RC beams with FRP transverse rebar using both existing equations and the proposed equation, we analyzed a total of 105 tests from the following sources: Tottori and Wakui [33], Nagasaka et al. [34], Maruyama and Zhao [35], Okamoto et al. [36], Nakamura and Higai [37], Zhao et al. [38], Maruyama and Zhao [39], Vijay et al. [40], Alsayed et al. [29], Duranovic et al. [41], Alsayed [42], Shehata et al. [43], Niewels [44], Ahmed et al. [45], Said et al. [46], Vora and Shah [47]. In this study, the shear strength of the numerical models is found to be below 500 kN. These raises concern that the proposed prediction model may yield inaccurate results for experimental data exceeding 500 kN in shear force. Therefore, the experimental data used in this study were specifically chosen from a dataset where the ultimate shear force was less than 500 kN. The prediction model available in TS-500 [19] is presented for medium and low strength concretes. Therefore, samples with compressive strength of concrete above 50 MPa are not included in this study. In addition, the experimental database used in the study was selected with transverse reinforcement ratio below 1.07% and a/d ratio below 4 from the experimental database in the literature. In addition, minimum r_b/d_b was assumed to be 3 [15]. Cover concrete and aggregate size were not reported in some experimental data. When these data were not reported in the literature, these values were accepted as 25 mm and 15 mm, respectively. A statistical summary of experimental database is presented in Table 3.

Table 3 Statistical evaluation of shear strength experimental database for RC beams with FRP stirrups

Property	Minimum	Maximum	Median	Mean	CoV (%)
b_w (mm)	120	300	200	202	24.66
d (mm)	210	600	260	291.48	24.49
a/d ratio	1.2	3.3	2.5	2.45	24.54
f_c (MPa)	19.6	50	34.9	36.05	17.13
r_f (%)	0.55	3.65	1.37	1.51	46.83
E_f (GPa)	29	200	58	71.9	50.4
r_{fw} (%)	0.04	1.07	0.35	0.43	75.23
E_{fw} (GPa)	30	144	58	70.46	51.32
f_{fwu} (MPa)	322	2040	891	1002.7	36.55
V_{exp} (kN)	49	440	113	148.59	58.53

3 Results and discussion

The principal stresses from the numerical models were examined. The visuals of the principal tensile and compressive stress contours and crack patterns of the M1-0.29-0.27 model from the moment just before cracking, the first cracking moment and the ultimate state are presented in Fig. 8. The principal compressive and tensile stress distributions of RC beams with GFRP transverse rebars were determined to be similar to the isostress distributions in conventional RC beams until first tensile cracks occur (Fig. 8(a)). However, it is observed that multiple bending cracks occur during the initial crack formation in the GFRP-reinforced beam, in contrast to the conventional RC beam (Fig. 8(b)). This phenomenon is thought to be a result of the reduced flexural stiffness in the RC beam with GFRP rebars compared to the steel-reinforced RC beam. Nevertheless, as the load continues to increase, the number of diagonal tensile cracks also increases (Fig. 8(c)). This indicates that the element has reached its ultimate state due to shear failure.

In the GFRP-reinforced beam, it is observed that stresses increase rapidly in the transverse rebars until the ultimate state is reached after the first tensile crack occurs, similar to RC beams with steel rebars (Fig. 9(a)). The maximum tensile stress of the longitudinal tensile rebar was 275.7 MPa when the first crack occurred in the concrete (Fig. 9(b)). Furthermore, the rebar tensile stress increased to 632.5 MPa, representing an approximate 129% increase when the beam reached the ultimate state (Fig. 9(c)). The maximum tensile principal stress in the transverse rebar also increased at the same rate, from 61.3 MPa to 140.6 MPa. Given the assumption made in creating numerical models, which is that GFRP rebars are not stressed under compressive forces, it has been determined that there is no compressive stress in the GFRP rebar placed in compression zones.

For the purpose of this research, all numerical models were designed in such a way that shear failure occurred. In reinforced concrete beams without stirrups, the shear failure mechanism is typically classified into three categories based on the shear span to effective depth ratio (a/d). When the a/d ratio falls within the range of approximately 2.5-6, the failure is attributed to Diagonal-Tension Failure (DTF).

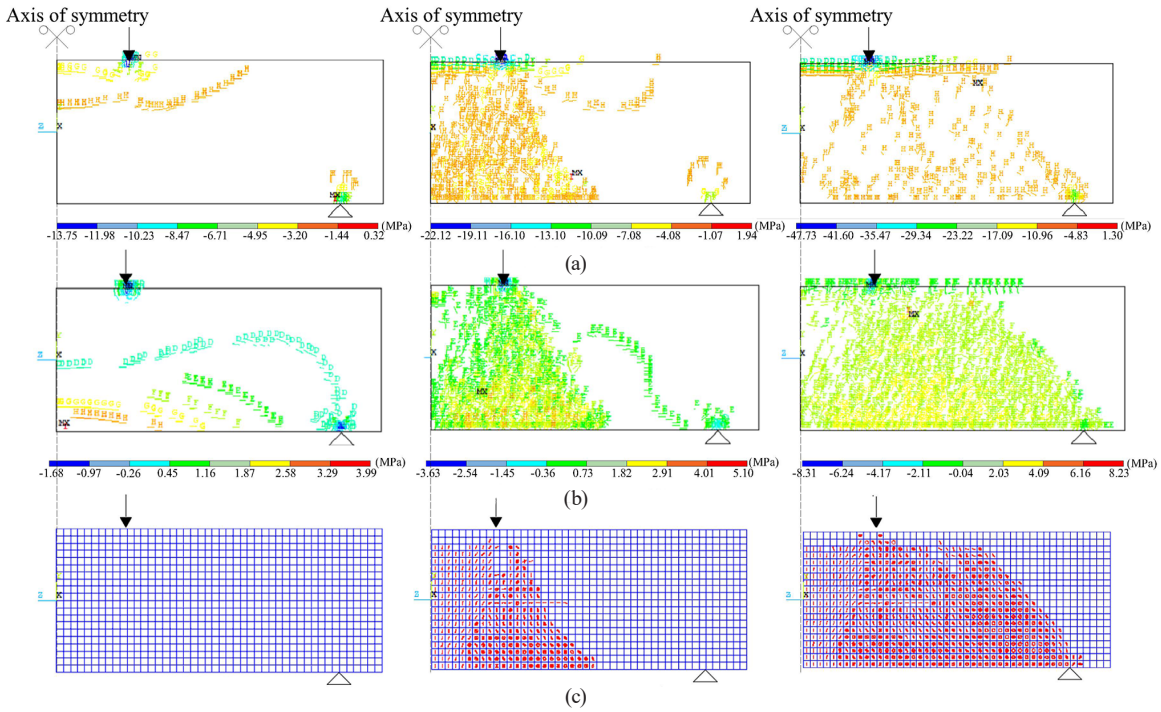

Fig. 8 Crack pattern at different load steps for M1-0.29-0.27 model, (a) Principal tensile stress, (b) Principal compressive stress, (c) Tensile crack

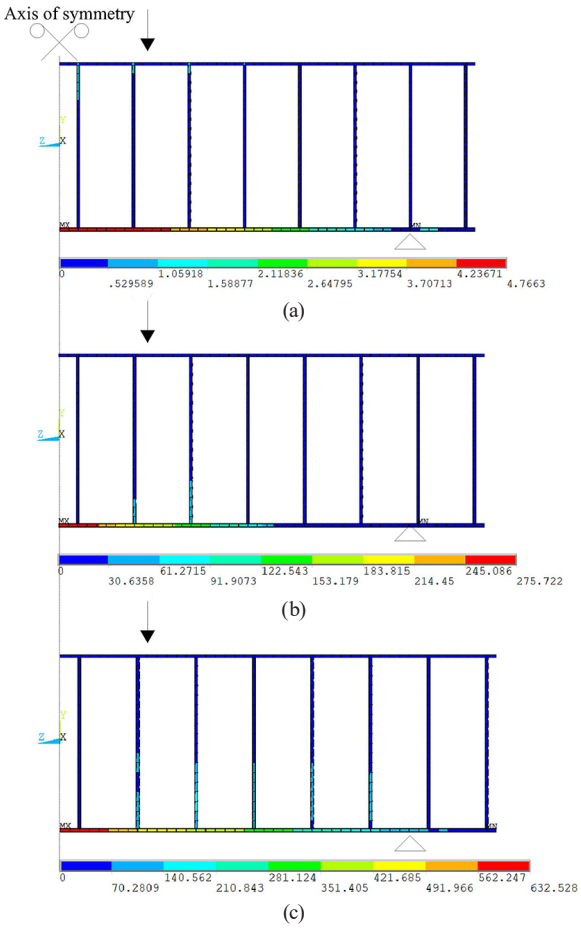

Fig. 9 Stress distributions in the GFRP rebar of the M1-0.29-0.27 model at different load steps, (a) Condition just before cracking in concrete, (b), The state of the first crack in the concrete, (c) Ultimate state

However, when the *a*/*d* ratio is within the range of approximately 1-2.5, the failure can be attributed to either Shear-Compression-Failure (SCF) or Shear-Tension Failure (STF) [48]. When the *a*/*d* ratio drops below 1.0, the beam exhibits its behavior similar to that of an arch with a tie-rod. In the case of RC beams with stirrups, concrete typically cracks first (Fig. 8(b)), and the rebar doesn't experience significant tensile stress until the concrete has cracked (Fig. 9(a)). Subsequent to the initial concrete crack, the stirrups bear the majority of the diagonal tensile stresses (Fig. 9(b)). As a result of the analysis of the numerical model of 27 RC beams with stirrups, it was determined that diagonal cracking occurred in the concrete first in the beams. It has been determined that in the zones where the concrete cracks, the stirrups limit the crack and take stress until the failure. In all models, stirrup failure was observed when it reached its ultimate strain. It was determined that the failure occurred in the mode of Diagonal-Tension-Failure (DTF) as the diagonal crack progressed. In a study conducted by Said et al. [46] on RC beams with an *a*/*d* ratio of 2 and normal concrete strength, and with a transverse rebar amount below 0.61%, the failure mode observed was Diagonal-Tension-Failure (DTF). In the research by Vora and Shah [47], it was found that failure occurred with either DTF or Stirrups-Rupture-Failure (SRF) in specimens with an *a*/*d* ratio of 1.79 and transverse reinforcement ratio below 0.25%. In the context of this study, the numerical models

of RC beams with stirrups had *a/d* ratios ranging from 1.11 to 1.58 and transverse reinforcement ratios from 0.17% to 0.40%. This indicates that the failure mode observed in this study was similar to the findings in the studies by Said et al. [46] and Vora and Shah [47].

The proposed equations (Eq. (12) and Eq. (15)) were compared with experimental results from the literature from various perspectives. The variation in results, regarding changes in shear strength based on section width (b_w), was examined for the results calculated using the proposed prediction model (V_{prep}) and the experimental results (V_{exp}) (Fig. 10(a)). It's evident that as the section width increases, the results become aligned more closely. For instance, at a section width of 150 mm, there is a 27.2% difference, while at a section width of 300 mm, this difference decreases to 4.7%. This can be interpreted as increased compatibility between the proposed prediction model and the experimental results with an increase in section width. One reason for this may be the fact that the numerical models used to refine the prediction models had widths of 250 mm and 300 mm.

Furthermore, it's worth noting that although the proposed prediction model and the numerical models did not account for changes due to aggregate size, the size effect of the aggregate may have played a role in the experimental results.

Changes in section effective depth (d) are examined in Fig. 10(b). It was determined as 87.2 kN, 221.5 kN and 355.8 kN for 200 mm, 400 mm and 600 mm section depths in linear slope line for V_{exp}, respectively. In contrast, for V_{prep}, these values were 88.6 kN (1.6% increase), 171.4 kN (29.2% decrease), and 251.4 kN (41.5% decrease), respectively. It can be interpreted that both the experimental results and the proposed prediction model provide less

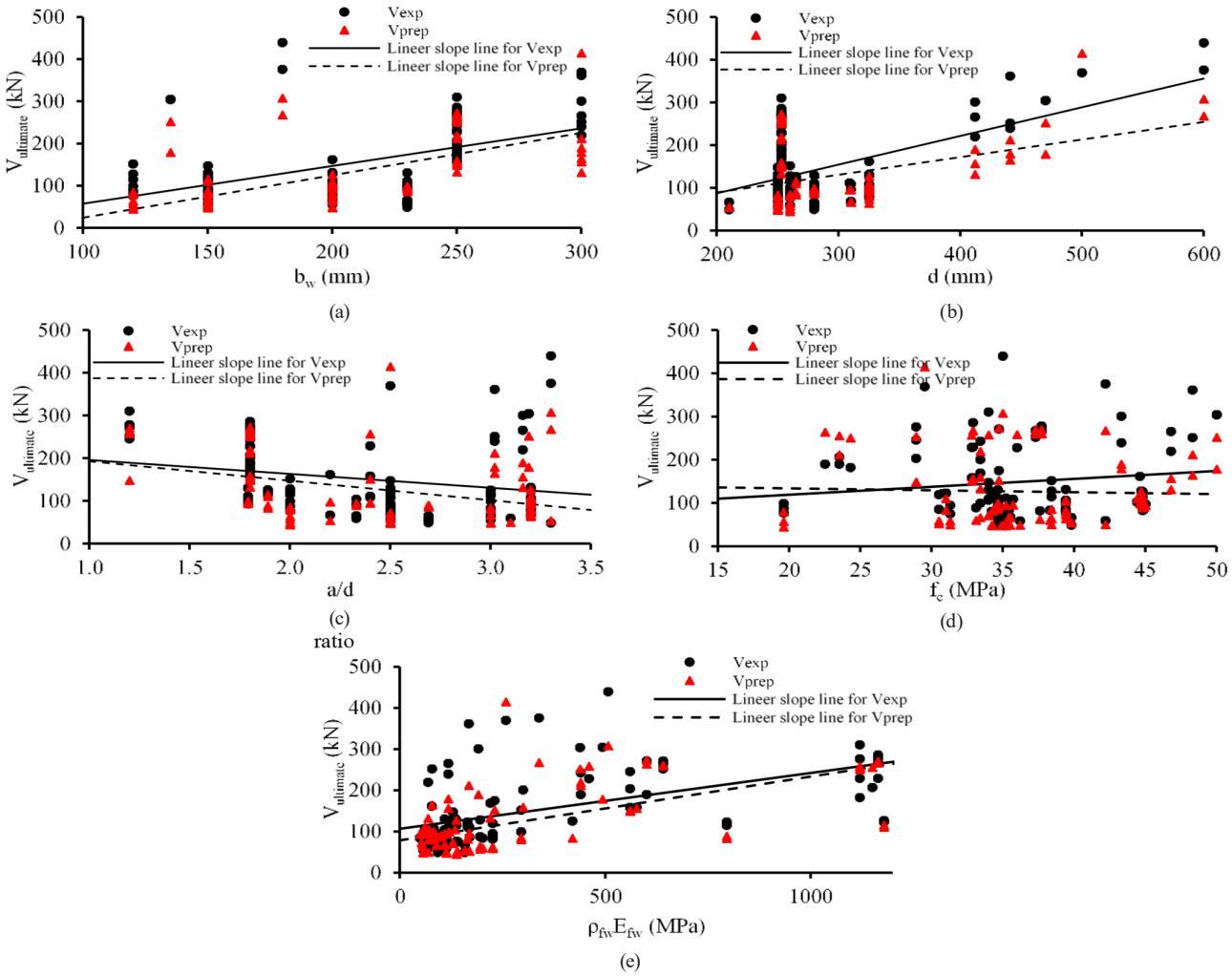

Fig. 10 Variation of experiment and proposed prediction model results according to different parameters; (a) variation according to the section width, (b) variation according to the section effective depth, (c) variation according to the shear span to effective depth ratio, (d) variation according to concrete strength, (e) variation according to the transverse rebar ratio and the product of Young's Modulus of the transverse rebar

erroneous results for sections with an effective depth of less than 500 mm. However, it can be noted that they yield conservative results for all effective depths.

Changes based on *a*/*d* ratio are examined in Fig. 10(c). Considering the linear slope line, shear strengths obtained from both the experimental and proposed prediction model for RC beams with an *a*/*d* ratio of 1 were determined as 196.2 kN and 193.0 kN, respectively. It has been determined that result of the experimental data for this RC beam with *a*/*d* ratio of 1 is 1.6% more than the proposed prediction model. As the *a*/*d* ratio increases, the error of the proposed prediction model also increases. This is due to the fact that the /d ratio in the numerical models used for revising the proposed prediction model falls in the range of 1.11–1.58. Nevertheless, it can be concluded that the proposed prediction model yields conservative results for all *a*/*d* ratios.

The change of the shear strength specified with proposed prediction model and experimental results according to the compressive strength of concrete (f_c) is analyzed in Fig. 10(d). For concrete with a compressive strength of 20 MPa, the shear strengths determined from the experimental data and the proposed prediction model, considering the linear slope line, were found to be 119.0 kN and 133.5 kN, respectively, revealing a difference of approximately 10.8% between the experimental data and the prediction model. The test result and the proposed equation yielded identical results at a compressive concrete strength of 26.5 MPa. However, at a concrete compressive strength of 50 MPa, the shear strength was determined to be 120.4 kN in the proposed prediction model, while it was observed to be 174.3 kN in the experimental data for the linear slope line. This indicates an approximate 30.9% difference between the experimental data and the proposed prediction model. Nonetheless, it can be concluded that the proposed prediction model yields conservative results for concrete compressive strengths exceeding 26.5 MPa.

The variation in shear strength based on $\rho_{fw}E_{fw}$ is illustrated in Fig. 10(e). At a $\rho_{fw}E_{fw}$ value of 300 MPa, on the linear slope line, the shear strength determined from the experimental data was 146.7 kN, whereas the shear strength calculated from the proposed prediction model was 124.4 kN. This discrepancy amounts to approximately 15.3%, with the experimental database being higher than proposed prediction model. However, this deviation reduces to 1.8% at a $\rho_{fw}E_{fw}$ value of 1200 MPa. It was also observed that as $\rho_{fw}E_{fw}$ increased, the experimental results became more consistent with the proposed prediction model.

The proposed shear strength prediction model is compared with various other prediction models, such as JSCE [11], BISE-99 [12], CSA S806-02 [13], CNR DT203 [14], ACI440.1R-106 [15], ISIS-M03-01 [16], Nehdi et al. [17], Fico et al. [7], Hegger et al. [18], CAN/CSA S806-12 [8], CSA S6-14 [10], Oller et al. [6], Valivonis et al. [9]. This comparison is conducted using a test database of 105 cases presented in the literature. A summary of the statistical evaluation of ratio of the shear strengths obtained from the experiments in the literature to the shear strengths from different prediction models ($\lambda = V_{exp}/V_{prep}$) is presented in Table 4. CoV, representing the Coefficient of Variation, is used as an indicator of variability. The χ factor serves as a general performance indicator, expressing the slope of the linear regression line obtained through

Table 4 Summary of statistical analysis of different shear strength prediction models

V_{exp}/V_{prep}	Mean	Median	Minimum	Maximum	CoV (%)	AAE (%)
Proposal	1.25	1.20	0.57	2.29	27.27	23.71
JSCE [11]	3.65	3.34	1.43	8.56	38.38	68.70
BISE-99 [12]	1.86	1.82	0.83	3.99	33.83	41.49
CSA S806-02 [13]	1.43	1.42	0.63	2.66	25.13	29.74
ACI 440.1R-06 [15]	1.73	1.71	0.58	3.86	35.37	39.46
CNR DT203 [14]	0.90	0.89	0.39	1.74	28.14	29.44
ISIS-M03-01 [16]	3.88	3.55	1.51	9.86	42.42	70.03
Nehdi et al. [17]	1.22	1.19	0.53	2.24	27.17	22.62
Fico et al. [7]	1.00	0.96	0.29	1.93	31.99	30.95
Hegger et al. [18]	1.21	1.18	0.42	2.09	27.00	24.80
CAN/CSA S806-12 [8]	1.77	1.67	0.62	3.96	35.68	39.62
CSA S6-14 [10]	1.85	1.74	0.78	3.98	34.01	41.42
Valivonis et al. [9]	1.78	1.67	0.76	3.94	31.66	40.19
Oller et al. [6]	1.19	1.14	0.55	2.37	29.48	21.25

the analysis. Shear strength prediction values (V_{prep}) were calculated for all prediction models and their ratio with the test results was determined ($\lambda = V_{exp}/V_{prep}$). The determined λ value was then categorized according to the modified Demerit Points Classification (DPC) system proposed by Collins [49] (Table 5). In this scoring system, a penalty value is assigned to each interval. The total weight value, determined by the penalty, reflects the overall performance of the prediction model. The penalty value is a weighting factor that takes into account accuracy, economy and safety [49, 50]. The product of the penalty and λ value represents the weight for that classification. The model with the lowest total weight value corresponds to the model with the best performance.

The accuracy of the proposed models is directly linked to the λ value (The graphical representation of 5 of the 14 prediction models that were statistically evaluated is presented in Fig. 11.). It has been observed that the model proposed by CNR DT203 [14] exhibits the narrowest range of λ values. Following closely is the model proposed by Fico et al. [7]. In these models, the maximum and minimum λ value ranges are 1.74-0.39 and 1.93-0.29, respectively. However, despite the narrow range of variation in the prediction models proposed by CNR DT203 [14] and Fico et al. [7], it has been determined that the mean and median values of them remain on the rather unsafe side. The prediction model proposed in this study, with values ranging from 2.29 to 0.57.

The four models demonstrating the best performance in terms of CoV values are CSA S806-02 [13], Hegger et al. [18], Nehdi et al. [17], and the proposed prediction model, respectively. The fact that the CoV value determined in the proposed prediction model are higher than the specified models does not mean that the model exhibits lower performance. CoV values are directly related to the mean value, which can lead to misinterpretation. Therefore, evaluating the models based on χ factors can provide a clearer assessment of the accuracy of the relationships between the experimental database and the prediction models. In the correlation relationship depicted in Fig. 11, the curve with a 450 angle represents a 0% tolerance (V_{exp}/V_{prep}) between the experimental results and the prediction models. The χ factor is the value that best quantifies the deviation from these relationships. Among the three models with the best χ factor values, which tend to favor safety, are the prediction model recommended by ACI 440.1R-06 [15], the proposed prediction model in the study, and the prediction model proposed by Oller et al. [6]. In addition to these statistical expressions, AAE values were also examined. AAE stands for Average Absolute Error and can be calculated using Eq. (17). Notably, the two models with the lowest AAE values among the prediction models were Oller et al. [6] with 21.3% and Nehdi et al. [17] with 22.6%, respectively. Following closely is the prediction model proposed in this study with an AAE of 23.7%. It can be said that these three models are the models with the lowest AAE. Furthermore, it becomes evident that most regulations [8, 10–13, 16] tend to favor safety in shear strength calculations. On the other hand, it is notable that the prediction models presented in the literature exhibit better consistency with the experimental database compared to the prediction models outlined in regulations other than ACI 440.1R-06 [15]. This divergence can be attributed to the fact that regulations typically incorporate safety factors in their designs.

Table 5 Modified Version of the Demerit Points Classification (DPC)

λ	Classification	Penalty
< 0.50	Extremely dangerous	10
0.5–0.85	Dangerous	5
0.85-1.15	Appropriate safety	0
1.15–2.00	Conservative	1
≥ 2.00	Extremely conservative	2

$$AAE = \frac{1}{n}\sum \frac{\left|V_{exp} - V_{prep}\right|}{V_{exp}} \times 100 \quad (17)$$

The histogram curve depicting the λ factor is presented in Fig. 11. λ factors for each prediction model were determined, and performance values based on the DPC were calculated (Tables 6 and 7). Notably, the best performance is exhibited by the proposed prediction model.

Following this model are Nehdi et al. [17], Valivonis et al. [9], and Hegger et al. [18]. The performance of these four prediction models is better than of the prediction models recommended by the regulations. Among the regulations, the three models that demonstrate the best performance according to the DPC system are CSA S806-02 [13], ACI 440.1R-06 [15], and BISE-99 [12]. JSCE [11] and ISIS-M03-01 [12] regulations seem to underperform compared to the proposed model. Specifically, when assessing safety ranges, 36.2% of the proposed prediction model falls within the appropriate range, whereas it's 12.4% for CSA S806-02 [13], which is the best-performing prediction model among the regulations. However, this percentage increases to 38.1% for Nehdi et al. [17], which demonstrates the best performance among the prediction models

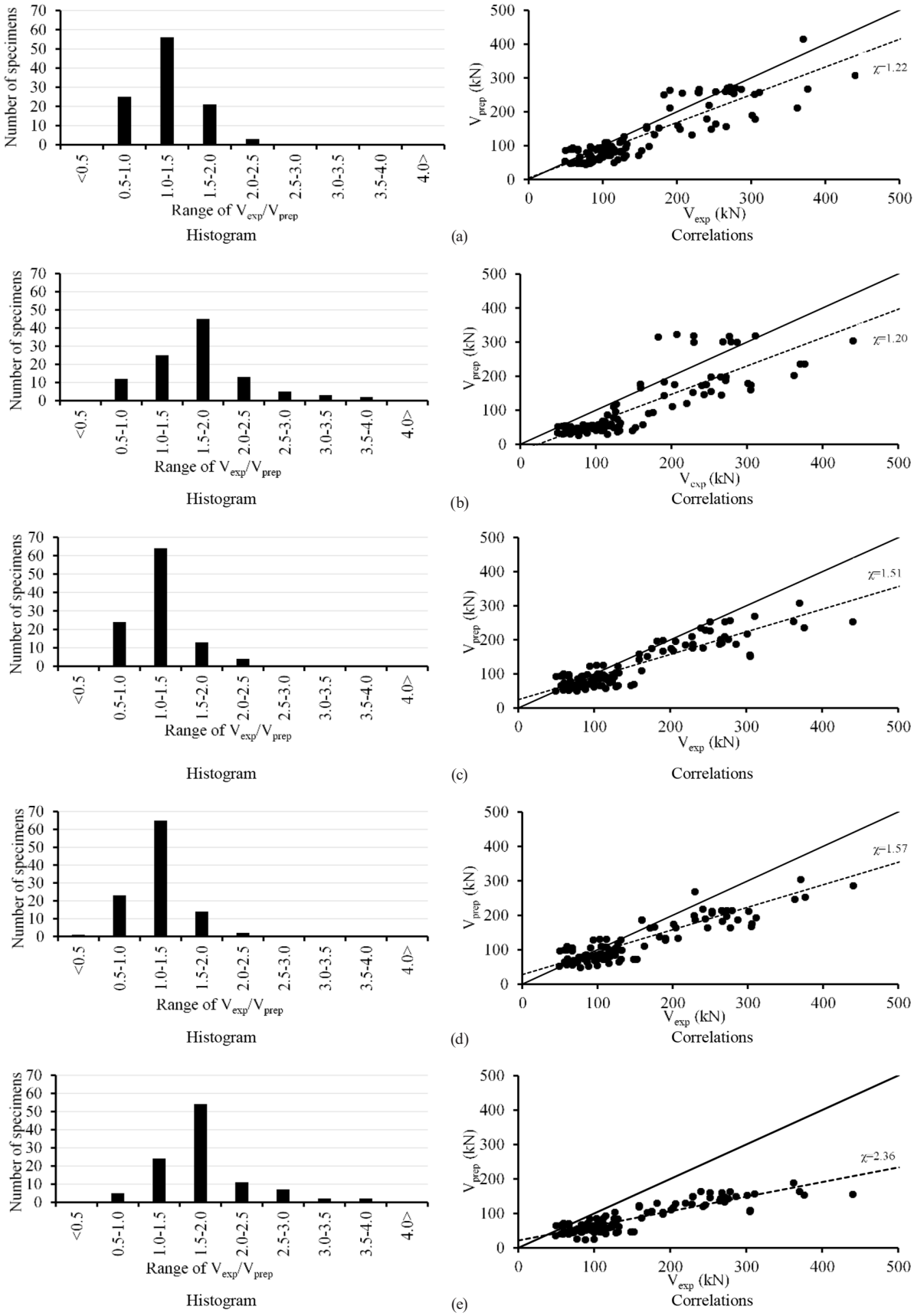

Fig. 11 Shear strength results according to different prediction models; (a) The proposed prediction model, (b) ACI 440.1R-06 [15], (c) Nehdi et al. [17], (d) Hegger at el. [18], (e) Valivonis et al. [9]

Table 6 Performance of different prediction models according to modified version of DPC (1)

λ	Penalty	Proposal	JSCE [11]	BISE-99 [12]	CSA S806-02 [13]	CNR DT203 [14]	ACI 440.1R-06 [15]	ISIS-M03-01 [16]
< 0.50	10	0	0	0	0	6	0	0
0.5–0.85	5	9	0	1	6	36	4	0
0.85–1.15	0	38	0	10	13	50	14	0
1.15–2.00	1	55	8	63	80	13	64	11
≥ 2.00	2	3	97	31	6	0	23	94
Total of weight		106	202	130	122	193	130	199

Table 7 Performance of different prediction models according to modified version of DPC (2)

λ	Penalty	Nehdi et. al. [17]	Fico et. al. [7]	Hegger et. al. [18]	CSA S806-12 [8]	CSA S6-14 [10]	Valivonis et al. [9]	Oller et al. [6]
< 0.50	10	0	5	1	0	0	0	0
0.5–0.85	5	10	29	11	3	2	12	3
0.85–1.15	0	40	41	35	10	8	46	4
1.15–2.00	1	51	30	56	65	63	42	76
≥ 2.00	2	4	0	2	27	32	5	22
Total of weight		109	175	120	134	137	112	135

proposed in the literature. Fico et al. [7] yielded favorable results in the statistical evaluation, but the overall performance does not align with these results. In these prediction models, it's noteworthy that 27.6% of the λ values remain at dangerous. In this case, the danger level increases the penalty score and therefore the total performance value decreases. As a result, the concrete contribution recommended in TS-500 [19] for the shear strength of conventional RC beams can be used by revising it for RC beams with FRP rebar (Eq. (12)). For these beams, the stirrup contribution suggested in TS-500 [19] can be revised by limiting the stress level for RC beams with FRP rebar (Eq. (15)). As with the shear strength prediction model of conventional RC beams, the shear strength prediction model of RC beams with FRP rebar can be calculated by adding the concrete shear strength contribution given in Eq. (12) and the stirrup shear strength contribution given in Eq. (15). According to the modified DPC proposed by Collins [49], the prediction model proposed in this study outperforms the models suggested in the literature and the regulations. This shows that more accurate calculations can be made by using the prediction model proposed for use in the shear design of RC beams with FRP stirrups calculated using Eqs. (12) and (15).

4 Conclusions

The shear strength equations given for steel rebar in TS-500 [19] have been developed with an analytical study, revised to make them usable for FRP rebar, and presented as a proposal. The following conclusions can be drawn as a result of the research.

- Similar to conventional RC beams, the FRP rebar did not receive tensile stress too much until tensile crack occurrence.
- The tensile stress distribution in RC beams with transverse and longitudinal GFRP rebar, with tendency to shear failure under four-point bending test, shows a stress distribution similar to the isostress distributions in conventional RC beams until the occurrence of the first crack in the concrete.
- The low Young's Modulus of the GFRP rebar caused the stiffness of the RC beams produced using these rebars to be low. For this reason, sudden displacements occurred in these beams as the first crack was formed. Thus, multiple bending cracks occurred during initial tensile crack formation.
- The failure mode is determined as DTF in GFRP-reinforced beams having 1.11-1.58 /d ratio, and 0.17-0.40% transverse reinforcement ratio.
- The prediction model used in TS-500 [19] for determining the concrete contribution in the shear strength of conventional RC beams were revised and proposed (Eq. (12)) for RC beams with FRP rebar.
- The prediction model used in TS-500 [19] that determine the stirrups contribution in the shear strength RC beams should be revised by limiting the ultimate stress level in the transverse FRP rebar (Eqs. (15) and (16)).

- The differences between the results obtained from the prediction models proposed by the regulations and the results obtained from the model proposed in the study is due to the tendency of the regulations to remain on the safe side.
- It has been determined that the proposed prediction model has the best performance compared to the modified version of DPC according to the current results.
- It is recommended that the proposed model be supported and developed by extensive laboratory studies in addition to current validations.

Nomenclature

α: Shear span
A_f: Total cross-sectional area of longitudinal rebar
A_w: Total cross-sectional area of shear rebar
b_w: The section width
c: Distance from extreme compression fiber to the neutral axis
C: Compressive force
d: The effective depth
d_b: Diameter of rebar
d_v: Effective depth of section in shear
E_c: Young's Modulus of the concrete
E_f: Young's Modulus of tensile rebar
E_{fw}: Young's Modulus of the shear FRP rebar
E_s: Young's Modulus of the steel rebar
f: The stress corresponding to each strain
f_c: The compressive strength of concrete
f_{ct}: The tensile strength of concrete
f_{fb}: Strength of bent portion FRP rebar
f_{fw}: Limiting stress in FRP stirrup to be used in design
f_{fwu}: Tensile strength of FRP stirrup
f_{fu}: Tensile strength of FRP
f_{yw}: Yield stress in steel stirrup to be used in design
h: The depth
L: Free length of specimen (length between anchors)
L_a: Anchor length
n: Number of elements
r_b: Internal radius of bend
s: Slip
s_{max}: The slippage corresponding to the maximum shear stress
s_s: Transverse rebar spacing
V_a: Shear stregth due to aggregate interlocking
V_c: Shear strength of concrete
V_{exp}: The shear strength obtained from the experiment
V_{fw}: The shear strength of the FRP stirrup
V_l: Shear strength of longitudinal rebar due to dowel action
V_{num}: The shear strength obtained from numerical model
V_{prep}: The shear strength obtained from prediction model
V_r: Shear strength of RC beam
V_t: The residual tensile strength existing between inclined cracks
V_w: Shear strength of transverse rebar
t: Steel tube thickness
T: Tensile force
ε: The strain
ε_0: The strain corresponding to the maximum stress of unconfined concrete
e_{fw}: Design value of shear rebar strain in ultimate limit state
λ: Evaluating factor between Vexp/Vprep
μ: The correction factor for FRP rebar
ρ_f: Longitudinal reinforcement ratio
ρ_{fw}: Transverse reinforcement ratio
τ: Bond strength
τ_{max}: Maximum bond strength
χ: General performance indicator that expresses the slope of the linear line obtained as a result of linear regression analysis

References

[1] Yuksel, I., Sakcalı, G. B. "Effects of reinforcement corrosion on reinforced concrete buildings", Proceedings of the Institution of Civil Engineers: Structures and Buildings, 175(3), pp. 244–258, 2021. https://doi.org/10.1680/jstbu.19.00111

[2] Esfandiari, J., Latifi, M. K. "Numerical Study of Progressive Collapse in Reinforced Concrete Frames with CFRP under Column Removal Numerical study of progressive collapse in reinforced concrete frames with FRP under column removal", Advances in Concrete Construction, 8(3), pp. 165–172, 2019. https://doi.org/10.12989/acc.2019.8.3.165

[3] Esfandiari, S., Esfandiari, J. "Simulation of the behaviour of RC columns strengthen with CFRP under rapid loading", Advances in Concrete Construction, 4(4), pp. 319–332, 2017. https://doi.org/10.12989/acc.2016.4.4.319

[4] Khaleel Ibrahim, S., Movahedi Rad, M. "Limited Optimal Plastic Behavior of RC Beams Strengthened by Carbon Fiber Polymers Using Reliability-Based Design", Polymers, 15(3), 569, 2023. https://doi.org/10.3390/polym15030569

[5] Szép, J., Habashneh, M., Lógó, J., Movahedi Rad, M. "Reliability Assessment of Reinforced Concrete Beams under Elevated Temperatures: A Probabilistic Approach Using Finite Element and Physical Models", Sustainability, 15(7), 6077, 2023. https://doi.org/10.3390/su15076077

[6] Oller, E., Marí, A., Bairán, J. M., Cladera, A. "Shear design of reinforced concrete beams with FRP longitudinal and transverse reinforcement", Composites Part B: Engineering, 74, pp. 104–122, 2015. https://doi.org/10.1016/j.compositesb.2014.12.031

[7] Fico, R., Prota, A., Manfredi, G. "Assessment of Eurocode-like design equations for the shear capacity of FRP RC members", Composites Part B: Engineering, 39(5), pp. 792–806, 2008. https://doi.org/10.1016/j.compositesb.2007.10.007

[8] Canadian Standards Association "CAN/CSA S806-12: Design and construction of building components with fibre reinforced polymers", Toronto, Canada, 2012.

[9] Valivonis, J., Budvytis, M., Atutis, M., Atutis, E., Juknevičius, L. "Study on shear resistance of fiberreinforced polymer-reinforced concrete beams", Advances in Mechanical Engineering, 7(7), pp. 1–17, 2015. https://doi.org/10.1177/1687814015593873

[10] Canadian Standards Association "CSA S6-14: Canadian highway bridge design code", CSA Group, Toronto, Canada, 2014.

[11] Japan Society of Civil Engineers "JSCE 1997: Recommendation for design and construction of concrete structures using continuous fiber reinforcing materials", Tokyo, Japan, 1997.

[12] British Institution of Structural Engineers "BISE-99: Interim guidance on the design of reinforced concrete structures using fiber composite reinforcement", London, UK, 1999.

[13] Canadian Standards Association "CSA S806-02: Design and construction of building structures with fibre-reinforced polymer", CSA Group, Toronto, Canada, 2002.

[14] Italian National Research Council "CNR-DT 203: Guide for design and construction of concrete structures reinforced with fiber-reinforced polymer bars", Rome, Italy, 2006.

[15] American Concrete Institute "ACI 440.1R-06: Guide for the design and construction of structural concrete reinforced with FRP bars", Farmington Hills, MI, USA, 2006.

[16] The Canadian Network of Centres of Excellence on Intelligent Sensing for Innovative "ISIS-M03-01: Reinforcing concrete structures with fibre reinforced polymers: Design manual", 2007.

[17] Nehdi, M., El Chabib, H., Saïd, A. A. "Proposed Shear Design Equations for FRP-Reinforced Concrete Beams Based on Genetic Algorithms Approach", Journal of Materials in Civil Engineering, 19(12), pp. 1033–1042, 2007. https://doi.org/10.1061/(ASCE)0899-1561(2007)19:12(1033)

[18] Hegger, J., Niewels, J., Kurth, M., "Shear analysis of concrete members with Fiber-Reinforced Polymers (FRP) as internal reinforcement", In: Proceedings of the 9th International Symposium of the Fiber-Reinforced Polymer Reinforcement for Reinforced Concrete Structures (FRPRCS-9), Sydney, Australia, 2009, pp. 1–8. ISBN: 9780980675504

[19] TSI "TS-500: Requirements for design and construction of reinforced concrete structures", Turkish Standards Institute, Ankara, Turkey, 2000.

[20] General Directorate for Foundations "TBEC-2018: Turkey Building Earthquake Code", 2018.

[21] American Society for Testing and Materials "ASTM D7205-11: Standard test method for tensile properties of fiber reinforced polymer matrix composite bars", ASTM, West Conshohocken, PA, USA, 2011. https://doi.org/10.1520/D7205_D7205M-06

[22] American Concrete Institute "ACI 440R-07: Report on fiber-reinforced polymer (FRP) reinforcement for concrete structures", Farmington Hills, MI, USA, 2007.

[23] "ANSYS" Swanson Analysis System Inc., 2013.

[24] Bangash, M. Y. H. "Concrete and concrete structures: Numerical modelling and applications", Elsevier Science Publishers Ltd., 1989. ISBN 1-85166-294-4

[25] Vint, L. "Investigation of bond properties of glass fibre reinforced polymer (GFRP) bars in concrete under direct tension", MSc Thesis, University of Toronto, 2012.

[26] Barris, C., Torres, L. I., Turon, A., Baena, M., Catalan, A. "An experimental study of the flexural behaviour of GFRP RC beams and comparison with prediction models", Composite Structures, 91(3), pp. 286-295, 2009. https://doi.org/10.1016/j.compstruct.2009.05.005

[27] Wolanski, A. J. "Flexural behavior of reinforced and prestressed concrete beams using finite element analysis", MSc Thesis, Marquette University, 2011.

[28] Ovitigala, T., Ibrahim, M. A., Issa, M. A. "Serviceability and ultimate load behavior of concrete beams reinforced with basalt fiber-reinforced polymer bars", ACI Structural Journal, 113(4), pp. 757–768, 2016. https://doi.org/10.14359/51688752

[29] Alsayed, S. H., Al-Salloum, Y. A., Almusallam, T. H. "Shear design for beams reinforced by GFRP bars", In: Non-metallic (FRP) reinforcement for concrete structures: Proceedings of the Third International Symposium (FRPRCS-3), Sapporo, Japan, 1997, pp. 285–297. ISBN: 4931451004

[30] Cladera, A., Marí, A., Bairán, J. M., Ribas, C., Oller, E., Duarte, N. "The compression chord capacity model for the shear design and assessment of reinforced and prestressed concrete beams", Structural Concrete, 17(6), pp. 1017–1032, 2016. https://doi.org/10.1002/suco.201500214

[31] Campana, S., Ruiz, M. F., Anastasi, A., Muttoni, A. "Analysis of shear-transfer actions on one-way RC members based on measured cracking pattern and failure kinematics", Magazine of Concrete Research, 65(6), pp. 386–404, 2013. https://doi.org/10.1680/macr.12.00142

[32] Canadian Standards Association "CAN/CSA S806-12: Design and construction of building components with fibre reinforced polymers", Toronto, Canada, 2012.

[33] Tottori, S., Wakui, H. "Shear capacity of RC and PC beams using FRP reinforcement", ACI Symposium Paper, 138, pp. 615–632, 1993. https://doi.org/10.14359/3944

[34] Nagasaka, T., Fukuyama, H., Tanigaki, M. "Shear performance of concrete beams reinforced with FRP stirrups", ACI Symposium Paper, 138, pp. 789–812, 1993.

[35] Maruyama, K., Zhao, W. J., "Flexural and shear behaviour of concrete beams reinforced by FRP rods", In: Corrosion and Corrosion Protection of Steel in Concrete, Sheffield Academic Press, 1994, pp. 1330–1339. ISBN: 1850757232

[36] Okamoto, T., Nagasaka, T., Tanigaki, M. "Shear capacity of concrete beams using FRP reinforcement", Journal of Structural and Construction Engineering, 455, pp. 127–136, 1994. (in Japanese) https://doi.org/10.3130/aijs.59.127_1

[37] Nakamura, H., Higai, T. "Evaluation of shear strength of concrete beams reinforced with FRP", Journal of Japan Society of Civil Engineers, 26, pp. 89–100, 1995. (in Japanese) https://doi.org/10.2208/jscej.1995.508_89

[38] Zhao, W., Maruyama, K., Suzuki, H. "Shear behavior of concrete beams reinforced by FRP rods as longitudinal and shear reinforcement", In: Non-Metallic (FRP) Reinforcement for Concrete Structures: Proceedings of 2nd International RILEM Symposium, Belgium, Ghent, 1995, pp. 352–359. ISBN: 9780419205401

[39] Maruyama, K., Zhao, W. "Size effect in shear behavior of FRP reinforced concrete beams", In: Proceedings of the 2nd International Conference on Advanced Composite Materials in Bridges and Structures (ACMBS-II), Montreal, Canada, 1996, pp. 227–234. ISBN: 9780921303640

[40] Vijay, P. V., Kumar, S. V., GangaRao, H. V. S. "Shear and ductility behavior of concrete beams reinforced with GFRP rebars", In: Proceedings of the 2nd International Conference on Advanced Composite Materials in Bridges and Structures (ACMBS-II), Montreal, Canada, 1996, pp. 217–226. ISBN: 9780921303640

[41] Duranovic, N., Pilakoutas, K., Waldron, P. "Tests on concrete beams reinforced with glass fibre reinforced plastic bars", In: Proceedings of the 3rd International Symposium on Non-metallic (FRP) Reinforcement for Concrete Structures (FRPRCS-3), Sapporo, Japan, 1997, pp. 479–486. ISBN: 4931451004

[42] Alsayed, S. H. "Flexural behaviour of concrete beams reinforced with GFRP bars", Cement and Concrete Composites, 20(1), pp. 1–11, 1998. https://doi.org/10.1016/S0958-9465(97)00061-9

[43] Shehata, E., Morphy, R., Rizkalla, S. "Fibre reinforced polymer shear reinforcement for concrete members: Behaviour and design guidelines", Canadian Journal of Civil Engineering, 27(5), pp. 859–872, 2000. https://doi.org/10.1139/l00-004

[44] Niewels, J. "Zum Tragverhalten von Betonbauteilen mit Faserverbundkunststoff-Bewehrung", (Load carrying behaviour of concrete members with fibre reinforced polymers), PhD Thesis, Aachen University, 2008.

[45] Ahmed, E. A., El-Salakawy, E. F., Benmokrane, B. "Shear performance of RC bridge girders reinforced with carbon FRP stirrups", Journal of Bridge Engineering, 15(1), pp. 44–54, 2010. https://doi.org/10.1061/(ASCE)BE.1943-5592.0000035

[46] Said, M., Adam, M. A., Mahmoud, A. A., Shanour, A. S. "Experimental and analytical shear evaluation of concrete beams reinforced with glass fiber reinforced polymers bars", Construction and Building Materials, 102, pp. 574–591, 2016. https://doi.org/10.1016/j.conbuildmat.2015.10.185

[47] Vora, T. P., Shah, B. J. "Experimental investigation on shear capacity of RC beams with GFRP rebar & stirrups", Steel and Composite Structures, 21(6), pp. 1265–1285, 2016. https://doi.org/10.12989/scs.2016.21.6.1265

[48] Samad, A. A. A., Mohamad, N., Ali, N., Jayaprakash, J., Mendis, P. "Rehabilitation of continuous reinforced concrete beams in shear by external bonding of carbon fiber reinforced polymer strips for sustainable construction", Key Engineering Materials, 708, pp. 49–58, 2016. https://doi.org/10.4028/www.scientific.net/KEM.708.49

[49] Collins, M. P. "Evaluation of shear design procedures for concrete structures", Report prepared for the CSA Technical Committee on RC Design, Canada, 2001.

[50] Moraes Neto, B. N., Barros, J. A. O., Melo, G. S. S. A. "Model to Simulate the Contribution of Fiber Reinforcement for the Punching Resistance of RC Slabs", Journal of Materials in Civil Engineering, 26(7), 2014. https://doi.org/10.1061/(ASCE)MT.1943-5533.0000913